AUTHOR QUERY FORM

ELSEVIER	**Journal: BBAMEM** **Article Number: 80125**	**Please e-mail or fax your responses and any corrections to:** **E-mail: corrections.essd@elsevier.spitech.com** **Fax: +1 61 9699 6721**

Dear Author,

Any queries or remarks that have arisen during the processing of your manuscript are listed below and highlighted by flags in the proof. Please check your proof carefully and mark all corrections at the appropriate place in the proof (e.g., by using on-screen annotation in the PDF file) or compile them in a separate list.

For correction or revision of any artwork, please consult http://www.elsevier.com/artworkinstructions.

Articles in Special Issues: Please ensure that the words 'this issue' are added (in the list and text) to any references to other articles in this Special Issue.

Location in article	Query / remark Please insert your reply or correction at the corresponding line in the proof
Uncited references: References that occur in the reference list but not in the text – please position each reference in the text or delete it from the list.	
Missing references: References listed below were noted in the text but are missing from the reference list – please make the list complete or remove the references from the text.	
	No query.

Electronic file usage
Sometimes we are unable to process the electronic file of your article and/or artwork. If this is the case, we have proceeded by:

☐ Scanning (parts of) your article   ☐ Rekeying (parts of) your article   ☐ Scanning the artwork

Thank you for your assistance.

Interactions at the bilayer interface and receptor site induced by the novel synthetic pyrrolidinone analog MMK3

C. Fotakis [a], S. Gega [a], E. Siapi [b], C. Potamitis [a,b], K. Viras [b], P. Moutevelis-Minakakis [b], C.G. Kokotos [b], S. Durdagi [b,c,d], S. Golic Grdadolnik [e], B. Sartori [f], M. Rappolt [f,*], T. Mavromoustakos [a,*]

[a] Chemistry Department, National and Kapodistrian University of Athens, Panepistimioupolis Zographou 15771, Greece
[b] Institute of Organic and Pharmaceutical Chemistry, National Hellenic Research Foundation, Vas. Constantinou 48, Athens 11635, Greece
[c] Department of Biology, Chemistry and Pharmacy, Free University of Berlin, 14195 Berlin, Germany
[d] Department of Biological Sciences, Institute for Biocomplexity and Informatics, University of Calgary, 2500 University Dr, Calgary, Canada T2N1N4
[e] Laboratory of Biomolecular Structure, National Institute of Chemistry, 1001 Ljubljana, Slovenia
[f] Institute of Biophysics and Nanosystems Research, Austrian Academy of Science, 8042 Graz, Austria

ABSTRACT

This work presents a thorough investigation of the interaction of the novel synthetic pyrrolidinone analog MMK3 with the model membrane system of dipalmitoylphosphatidylcholine (DPPC) and the receptor active site. MMK3 has been designed to exert antihypertensive activity by functioning as an antagonist of the angiotensin II receptor of subtype 1 (AT_1). Its low energy conformers were characterized by 2D rotating-frame Overhauser effect spectroscopy (ROESY) in combination with molecular dynamics (MD) simulations. Docking study of MMK3 shows that it fits to the AT_1 receptor as SARTANs, however, its biological activity appears to be lower. Thus, differential scanning calorimetry (DSC), Raman spectroscopy and small angle X-ray scattering (SAXS) experiments on the interaction of MMK3 with DPPC bilayers were carried out and results demonstrate that the drug is well incorporated into the membrane leaflets and furthermore causes partial bilayer interdigitation, although less effective than SARTANs. Thus, it appears that the nature of the bilayer matrix and the stereoelectronic active site requirements of the receptor are responsible for the low bioactivity of MMK3.

© 2009 Published by Elsevier B.V.

1. Introduction

The renin angiotensin system (RAS) constitutes the major system that regulates blood pressure. Therefore, it is the main target in the drug design for developing novel synthetic antihypertensive drugs. The first rationale behind the synthesis of novel angiotensin analogs was to block the formation of vasoconstrictive hormone angiotensin II (Ang II). Renin and angiotensin converting enzymes are responsible for transforming in the body angiotensinogen to angiotensin I (Ang I) and subsequently to Ang II. The blocking of angiotensin converting enzyme was crowned with success and the market experienced captopril and its congeners as beneficial molecules in blood regulation. However, their side effects of dry mouth and angioedema precluded them from being the ideal drugs for hypertension. Recently, the synthetic molecule aliskiren entered the market with trade name Tekturna (Novartis) and is the only available inhibitor from the renin inhibitor class [1].

The second class of synthetic molecules aims to block Ang II at the AT_1 receptor [2]. The first peptide analogs synthesized for this purpose, although not successful, provided molecular models for further rational drug design. To comprehend the stereoelectronic requirements for receptor binding, the stereochemical features of Ang II and its peptide antagonists sarmesin and sarilesin were explored [3–12]. These synthetic peptide analogues and other non-peptide AT_1 antagonists (commercially available and novel compounds) are designed to mimic the C-terminal part of Ang II. In this regard, losartan was the first successful peptidomimetic analog to be marketed. Furthermore, angiotensin receptor blockers (ARBs) have been developed to produce a more complete blockade of the action of angiotensin II as compared to other drug classes as well as decrease of their side effects [13–18].

Based on the molecular characterization of these antagonists, a new avenue was explored in an attempt to design and synthesize novel AT_1 antagonists. Thus, (5S)-1-benzylo-5-(1H-imidazol-1-ylo-methylo)-2-pyrrolidinone) denoted as MMK1 was synthesized to possess pyrrolidinone as template instead of biphenyltetrazole. However, MMK1 did not show the desired biological properties as the in vitro and in vivo studies demonstrated [19]. For this purpose, we proceeded with the synthesis of a derivative of MMK1, the (5S)-1-

* Corresponding authors. M. Rappolt is to be contacted at the Institute of Biophysics and Nanosystems Research, Austrian Academy of Science, 8042 Graz, Austria. Tel.: +39 040 375 8708; fax: +39 040 375 8029. T. Mavromoustakos, Chemistry Department, National and Kapodistrian University of Athens, Panepistimioupolis Zographou 15771, Greece. Tel.: +30 2107274293; fax: +30 2107274261, +30 2107274293.
E-mail addresses: michael.rappolt@elettra.trieste.it (M. Rappolt), tmavro@eie.gr (T. Mavromoustakos).

benzylo-5-(1H-benzimidazol-1-ylo-methylo)-2-pyrrolidinone named MMK3 (Fig. 1), which differs from MMK1 in two aspects: (a) it has a methoxy group at 11 position and (b) it contains a benzimidazole ring instead of a phenyl ring. The rationale behind these structural modifications was first to mimic in part the Ang II antagonist sarmesin (Sar) and second to extend the aromaticity of the molecule. We note, that the key requirement for antagonist activity of sarmesin is its methoxy group. In fact, the superagonist Sar[AngII] is identical to sarmesin except that it contains a methoxy group instead of phenolic hydroxyl group at Tyr[4]. Detailed synthesis of this molecule and biological data are reported elsewhere [20]. However, MMK3 as did MMK1, appeared not to have the desired activity both *in vitro* and *in vivo*. To some extent this was a surprising outcome, since the initial molecular modeling certified good binding properties of MMK3 with the active site of the AT_1 receptor [19, 20].

The cell membrane is believed to play an important role in the cause and progression of hypertension. On the basis of extensive studies of the antagonist losartan, our laboratory has proposed a two-step model, in which this antihypertensive drug is first incorporated into the bilayers through the lipid–water interface and then laterally diffuses to reach the active site of the AT_1 receptor [21]. A two-step mechanism has also been suggested for other amphiphilic molecules such as cannabinoids and calcium channel antagonists [22–25]. For the above reason it was decided to study the interaction of MMK3 with lipid model membranes.

The lowest energy conformer of MMK3 was derived from 2D ROESY data in combination with molecular modeling. Additionally, since new models of the AT_1 receptor have been published [26], we have re-examined the interactions of MMK3 in the receptor site, this time in a lipid environment by applying MD simulations. Then, in a second part the MMK3:bilayer interactions in great detail were characterized by analyzing differential scanning calorimetry (DSC), Raman spectroscopy and small angle X-ray diffraction experiments.

Hydrated DPPC lipids are used because they spontaneously form multilamellar bilayers whose dynamic and thermotropic properties have been extensively studied by various biophysical methods [27–36]. Moreover, phosphatidylcholines are the most abundant lipid species in sarcolemma cardiac membranes. The most frequently found among them are PCs with oleic and linoleic chains, and further DPPC [37]. Another study points out that partition coefficient of DPPC, especially in the fluid state, resembles that of natural cardiac membranes [38].

This allows to learn about the thermodynamic changes in the presence of MMK3, to determine chain fluidity and mobility alterations, and finally to correlate theses results with the structural modifications on a molecular level. A concrete model for partial bilayer interdigitation is presented and some potential scenarios in the framework of the two-step reaction model are discussed.

2. Materials and methods

2.1. Sample preparation

MMK3 was synthesized as described previously [19,20]. Lα-dipalmitoylphosphatidylcholine (Lα-DPPC, 99+%) was purchased from Avanti Polar Lipids Inc (Alabaster, AL) and spectroscopic grade $CHCl_3$ from Sigma Aldrich (St. Louis, MO). For nuclear magnetic resonance (NMR) measurements, the MMK3 concentration used was 10 mM dissolved in $CDCl_3$. For DSC measurements appropriate amounts of DPPC and MMK3 diluted in chloroform were mixed, dried under stream of N_2 and then stored under vacuum overnight. After dispersing in water (50% w/w), portions of the samples (*ca.* 5 mg) were sealed in stainless steel capsules obtained from Perkin-Elmer (Norwalk, CT). The same sample preparation was carried out for the Raman spectroscopy measurements. The amount of sample used was *ca.* 40 mg. For X-ray scattering experiments aqueous dispersions of multilamellar vesicles were prepared according to the above protocol

τ_1 = C5-N1-C6-C7
τ_2 = C3-C2-C13-N14
τ_3 = N1-C6-C7-C12
τ_4 = C2-C13-N14-C18
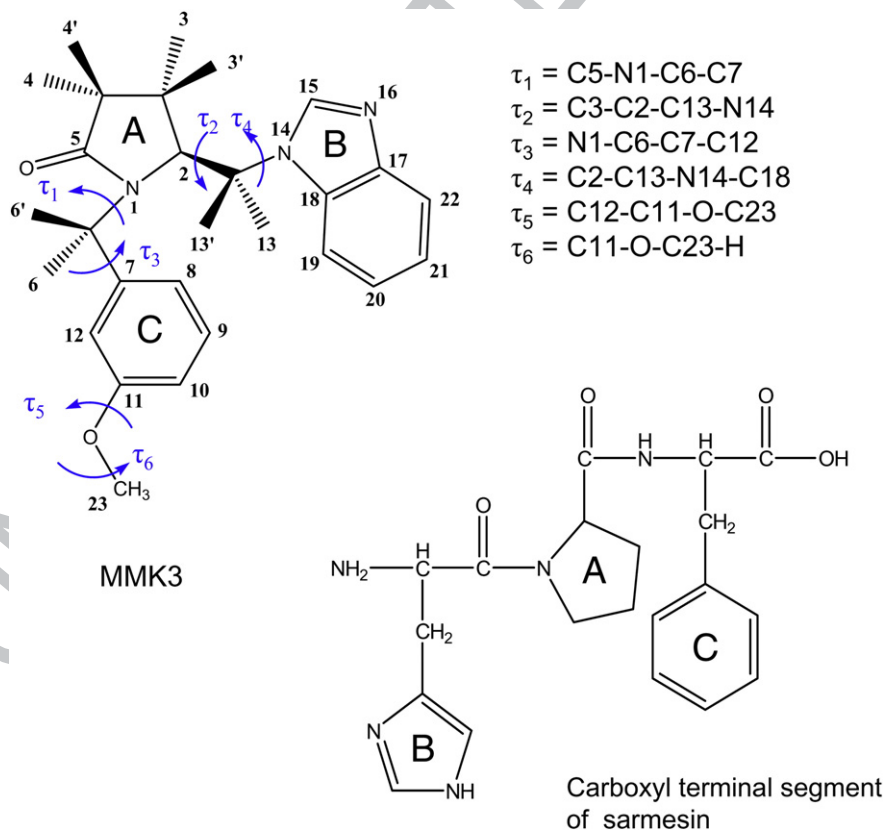τ_5 = C12-C11-O-C23
τ_6 = C11-O-C23-H

Fig. 1. Chemical structures of MMK3 and the carboxyl terminal segment of sarmesin. For MMK3 the critical dihedral angles that determine its conformational properties are defined. Equivalent aromatic rings of MMK3 and sarmesin are labeled with the same letters A–C.

with a final lipid weight concentrations of 25%. The drug concentrations used for the different experiments were $x = 0.01$ (99% molar ratio of phospholipid and 1% molar ratio of drug), $x = 0.05$ (95% molar ratio of phospholipid and 5% molar ratio of drug) and $x = 0.20$ (80% molar ratio of phospholipid and 20% molar ratio of drug).

2.2. NMR spectroscopy

NMR spectra were recorded on a Varian INOVA 600 MHz spectrometer (Palo Alto, CA) at 25 °C. The Double Quantum Filter Correlation Spectroscopy (DQF-COSY), Heteronuclear Single Quantum Coherence (^1H–^{13}C gHSQC) and Heteronuclear Multiple Bond Correlation (^1H–^{13}C gHMBC) were performed with pulsed field gradients. The offset compensated Rotating Overhauser SpectroscopY (ROESY) experiment was performed using a mixing time of 150 ms and a 4 kHz spin-locking field strength [39]. The ^1H and ^{13}C spectral windows used were 6000 Hz and 30,000 Hz, respectively. The homonuclear proton spectra were acquired with 4096 data points in t_2 dimension, 4–32 scans, 256–512 complex points in t_1 dimension and with a relaxation delay of 1–1.5 s. The ^1H–^{13}C heteronuclear experiments were acquired with 1024–4096 data points in t_2 dimension, 32–64 scans and 128–1024 complex points in t_1 dimension. Experimental data were processed using Varian VNMR software. Spectra were zero-filled two times and apodized with a squared sine bell function shifted by $\pi/2$ in both dimensions. Interproton distances were calculated from integrated and normalized cross-peak intensities in ROESY spectra. The distance between adjacent aromatic protons (2.46 Å) was used for calibration. The resulted distances were corrected for the frequency offset effects to be eliminated. Upper and lower limit constraints were estimated as $\pm 10\%$ of the resulted values.

2.3. Molecular mechanic (MM) conformational analysis studies

Molecular modeling analysis was performed on a Silicon Graphics O_2 workstation using QUANTA software (MSI, London, UK) and CHARMm force field. The dielectric constant (ε) was set to 1 to simulate $CDCl_3$ used in the NMR studies. The first step in the conformational analysis of MMK3 was to construct a preliminary 3D model which was minimized using the first order minimization algorithms, steepest descents, conjugate gradient, and Newton Raphson with 0.01 kcal/mol as the convergence criterion. This conformer was further subjected to random sampling obtaining 1000 low energy conformers. Cluster analysis led to 11 clusters using a dihedral angle RMSD threshold criterion. The lowest energy conformer of each cluster was further minimized. Among them, only three conformers satisfied the interatomic distances measured by the ROESY spectrum were selected.

2.4. "In silico" docking studies

Molecular docking simulations using the FlexX algorithm of SYBYL [40] have been employed to the three lowest energy conformers of MMK3 obtained by a combination of experimental and molecular modeling results. FlexX uses a fast docking method that allows flexibility in the ligands, keeping the receptor rigid, and it uses an incremental construction algorithm in order to place flexible ligands into a fully specified binding site. The default FlexX scoring function was used in the calculations. FlexX uses formal charges, which were turned on during docking.

2.5. Molecular dynamics (MD) simulations

MD simulations have been carried out in order to examine the stability of ligand inside the binding pocket, and understand the binding interactions between receptor and ligand.

The coordinate of the MMK3 ligand was submitted to PRODRG [41] algorithm to obtain Gromacs topologies. The DPPC lipid bilayers model for the MD simulations was taken from Karttunen [42] (it includes a 128 DPPC lipids and 3655 water molecules coordinate file derived from 100 ns MD simulations [43]). The MD simulations were performed with the GROMACS 3.3.1 software package [44] using the GROMOS96 force field [45]. Simulations were run in the NPT ensemble at 300 K and 1 bar with periodic boundary conditions. During equilibration the Berendsen barostat and thermostat algorithms [46] were applied. Electrostatic interactions were calculated using the particle mesh Ewald method [47]. Cutoff distances for the calculation of Coulomb and van der Waals interactions were 1.0 and 1.4 nm, respectively. Prior to the dynamics simulation, energy minimization was applied to the full system without constraints using the steepest descent integrator for 2000 steps with the initial step size of 0.01 Å (the minimization tolerance was set to 1000 kJ/(mol nm)). The system was then equilibrated via 250 ps simulation with a time step of 2 fs, subsequently a 2.5 ns simulation was performed at 300 K and 1 bar with a time step of 2 fs using the Berendsen thermostat [46] and Parrinello–Rahman barostat algorithms [48]. All bonds were constrained using the linear constraint solver (LINCS) algorithm [49]. Visualization of the dynamics trajectories was performed with the visual molecular dynamics (VMD) software package [50] and the Origin 6.0 program (OriginLab Corporation, Northampton, MA) was used for the plots.

2.6. Differential scanning calorimetry

Thermal scans were carried out using Perkin-Elmer DSC-7 calorimeter (Norwalk, CT). All samples were scanned from 10 to 60 °C until identical thermograms were obtained using a scanning rate of 2.5 °C/min. The temperature scale of the calorimeter was calibrated using indium ($T_m = 156.6$ °C) and DPPC bilayers ($T_m = 41.2$ °C). The following diagnostic parameters were used for the study of drug to membrane interactions: T_m (maximum of the recorded heat capacity), T_{onset} (the starting temperature of the phase transition) and $T_{m1/2}$ (the half-height width of the phase transition). An empty pan for the base line and a sample containing double distilled water were run for the temperature range of 10–60 °C as a reference for the background. This background was subtracted from each thermal scan of the samples. The area under the peak, represents the enthalpy change during the transition (ΔH). The mean values of ΔH of three identical scans were tabulated.

2.7. Raman spectroscopy

The Raman spectra were obtained with 4 cm^{-1} resolution from 3500 to 400 cm^{-1} with interval 2 cm^{-1} using a Perkin-Elmer NIR FT-spectrometer (Spectrum GX II, Norwalk, CT) equipped with CCD detector (Norwalk, CT). The measurements were performed at a temperature range of 27–50 °C. The laser power (a Nd:YAG at 1064 nm, Norwalk, CT) was controlled to be constant within 400 mW during the experiments. 1500 scans were accumulated and back scattering light was collected.

2.8. X-ray diffraction

Small angle X-ray scattering (SAXS) experiments were performed with a small- and wide angle X-ray scattering camera with Kratky collimation [51] (SWAXS, Hecus X-ray Systems, Graz, Austria) mounted on a sealed-tube generator (Philips PW 1729, Philips, Holland) operating at 2 kW. Cu-K_α radiation ($\lambda = 1.54$ Å) was selected using a tungsten filter. A linear one-dimensional position-sensitive detector (PSD 50-M, Hecus X-ray Systems, Graz, Austria) covered the q-range of interest from 0.004 to 0.5 Å^{-1}. For the measurements, the sample was transferred in a 1.5 mm capillary and measured at 25 and

261 50 °C, respectively. The same capillary filled with water was measured
262 as background. The exposure time was fixed to one hour and at each
263 temperature the sample was exposed 10 times.

264   After background subtraction the scattering patterns were ana-
265 lyzed by the global analysis program (GAP) [52]. For the lattice
266 contributions of the lamellar fluid phase the Caillé theory [53,54] and
267 for the gel phase the paracrystalline theory [55] were considered. For
268 the bilayer contribution a simple 4 parameter model was applied. This
269 model uses one Gaussian for the head-groups and another for the
270 hydrophobic core. A more detailed description of this model is given
271 in Pabst's recent review [56].

3. Results

3.1. Structure assignment and conformational analysis of MMK3

274   2D NMR COSY, ROESY, HSQC and HMBC experiments confirmed
275 the chemical structure of MMK3 given in Fig. 1. The ^{1}H and ^{13}C NMR
276 chemical shift assignments for ^{1}H and ^{13}C are given in Table 1. The
277 spectra of MMK3 are obtained at $CDCl_3$ environment which has a
278 lipophilic nature and simulates the lipophilic environment of lipid
279 bilayers. Although micelle and especially liposomes are more
280 commonly used mediums for simulating the lipid environment [57],
281 our previous studies had shown that AT_1 antagonists in $CDCl_3$,
282 micellar or liposomal environment adopt almost identical conforma-
283 tions [58]. These results justify in our present study the usage of the
284 deuterated chloroform solvent.

285   Structure elucidation of MMK3 was achieved based on the
286 published structure of MMK1 which as mentioned in the introduction
287 contains the identical ring A, the methylene bridge and ring C without
288 methoxy group [19]. MMK3 bears benzimidazole ring instead of
289 imidazole ring. Briefly, H15 is resonated at 7.26 ppm as a singlet like in
290 MMK1 [19]. Additionally, the 2D ROESY experiment allowed to
291 differentiate between H19/22 and H20/21, because H19/22 showed
292 ROE effect with H13/13′. The deshielded chemical shift values of H19/
293 22 relatively to H20/21 confirmed the ROE results. The protons of the
294 methoxy group are resonating as a singlet at 3.78 ppm. The easy
295 assignment of primary, secondary and tertiary carbon chemical shifts
296 was achieved using 2D HSQC experiment and quaternary carbons
297 using 2D HMBC experiment. The 2D ROESY experiment showed the
298 through space connectivities between vicinal spatial protons pre-

299 sented in Table 2. Among the observed ROEs the critical one is that
300 between 4′ and protons 20/21, because it determines the bend of the
301 molecule and the spatial vicinity between pyrrolidinone and
302 benzimidazole rings. In order to determine the lowest energy
303 conformers, compatible with the critical ROEs, first the molecule
304 was optimized using different energy minimization algorithms such
305 as steepest descents, conjugate gradient, and Newton Raphson until
306 $E_i - E_{i-1}$ was <0.001 kcal/mol. Random sampling was applied to find
307 even lower energy structures using only the critical ROE H4′-H20/21
308 as a constraint. The obtained different conformers were again
309 minimized using steepest descent and conjugate gradient algorithms
310 until $E_i - E_{i-1}$ was <0.001 kcal/mol and classified into clusters. Table 3
311 describes the average structures, defined as conformers A–C of three
312 clusters that are compatible with the ROE constraints. In conformer A
313 the rings of benzimidazole and phenyl are far away from each other. In
314 conformer B the two rings are almost perpendicular and in close
315 proximity to each other. The close proximity is preserved in
316 conformer C, but the two rings are almost parallel. These three low
317 energy conformers are docked in AT_1 receptor and the best scored
318 binding pose is shown in Fig. 2. Panel A in Fig. 2 shows the structural
319 details of MMK3 and the surrounding amino acids of the active site
320 while panel B focuses on the lipophilic profile of the active site. The
321 major characteristic of the docking is that benzimidazole ring is
322 surrounded by the lipophilic moieties of Val108, Leu112 and Trp253.
323 The carbonyl of pyrrolidinone is hydrogen bonded with Tyr113 and
324 the aromatic ring C is situated between the lipophilic aromatic rings
325 (shown in brown color) of PHE182 and TYR113. Interestingly, the
326 major part of the cavity that surrounds MMK3 is lipophilic, some bear
327 intermediate polarity (green color). Only barely in the depth of the
328 cavity a small hydrophilic segment is observable (blue color).

329   The best-docked complex among the three lowest energy
330 conformers was used as input in the MD simulations using the AT_1
331 receptor surrounded by a lipid bilayer environment. MMK3 keeps
332 identical conformation with that found in $CDCl_3$ and receptor active
333 site at lipid bilayers environment.

Table 1
Structure elucidation of MMK3. Chemical shifts obtained with ^{1}H and ^{13}C NMR spectra and ^{1}H-^{13}C couplings through HSQC and HMBC.

Proton	Chemical shift (ppm)	Carbon	Chemical shift (ppm)	HSQC	HMBC
3, 3′	1.85 (m), 2.09 (m)	3	21.13	H3, H3′	H4, H4′, H2, H13, H13′
4, 4′	2.39 m), 2.50 (m)	4	29.73	H4, H4′	H3′
2	3.63 (m)	2	55.26	H2	H3, H4, H13, H13′, H6
6, 6′	3.75 (d), 4.88 (d)	6	44.47	H6, H6′	H12, H8
23	3.78 (s)	23	55.25	H23	
13, 13′	3.95 (q), 4.02 (q)	13	68.91	H13, H13′	H3, H3′, H2
12	6.68 (s)	12	113.57	H12	H6, H6′, H8, H10
8	6.71(d)	8	120.26	H8	H6, H6′, H12, H10
10	6.80 (m)	10	113.24	H10	
9	7.20 (t)	9	130.05	H9	
19/22	7.74 (d)	19/22	127.93	H19/22	H20/21, H19/22
15	7.26 (s)	15	145.33	–	H19/22
20/21	7.37 (d)	20/21	130.06	H20/21	H20/21
		17/18	132.42	–	H20/21
		7	137.63	–	H6, H6′, H9
		11	159.97	–	H23, H12, H10, H9
		5	175.02	–	H3, H4, H4′, H2, H6, H6′

Table 2
Interproton distances of MMK3 as they were calculated from volumes of ROEs. Numbering used in the table is provided in Fig. 1.

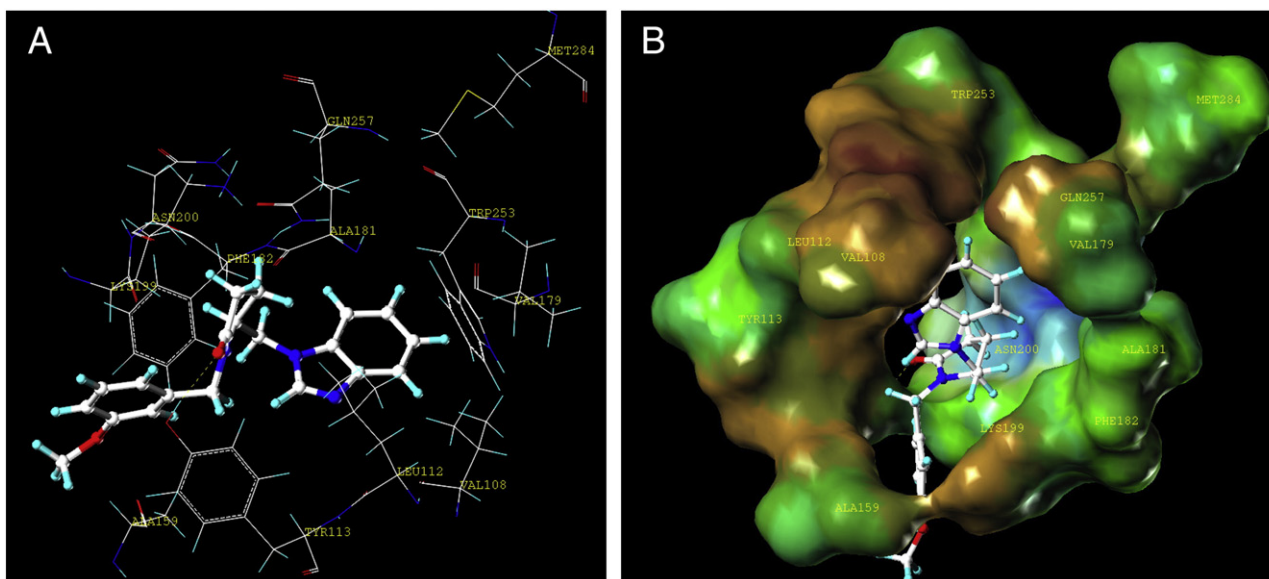| Protons	Distances ( )
H12–H6	2.40
H12–H6′	2.74
H8–H6	2.74
H8–H6′	2.40
H23–H10	2.81
H13–H2	1.89
H13′–H2	1.89
H13–H3	2.57
H13′–H3	2.69
H4′–H20/21	3.00
H13′–H19/22	3.47
H13–H19/22	3.18

Table 3
Values of dihedral angles (defined in Fig. 1) of low energy conformer of MMK3 and conformers A–C. Derived conformer A has a relative value of energy −32.3, conformer B −43.3 and conformer C −40.3 kcal/mol.

Dihedral angles	Values of dihedral angles (°) for the starting conformer	Values of dihedral angles (°) for conformer A	Values of dihedral angles (°) for conformer B	Values of dihedral angles (°) for conformer C
τ_1	101.4	77.6	85.6	−63.5
τ_2	−61.9	58.7	−152.4	60.9
τ_3	−67.6	−83.9	91.0	−89.3
τ_4	116.0	−107.0	65.1	−175.1
τ_5	173.4	5.6	−4.1	42.8
τ_6	−58.5	−64.4	−59.7	−68.6

Fig. 2. Docking of MMK3 in AT$_1$ receptor using different views. Panel A shows the structural details of MMK3 and the surrounding amino acids of the active site. Panel B focuses on the lipophilic profile of the active site. Colors of blue represent the hydrophilic, brown the lipophilic and green the intermediate polarity segments of the receptor active site. (For interpretation of the references to colour in this figure legend, the reader is referred to the web version of this article.)

A representative snapshot of the MD simulations is shown in the Fig. 3. The ligand (shown with bold sticks) at the active site of the receptor (yellow helices) was merged to DPPC and water molecules (shown with sticks). After the MD simulations, a conformational analysis was performed to six rotatable bonds (defined in the corresponding Fig. 1) in ligand. The torsional angle values of these six dihedral angles were screened throughout the MD simulations and showed to be stable.

Fig. 4A shows the conformations of MMK3 used as input coordinate for the ligand (derived from docking studies) before the MD simulations and panel B of Fig. 4 the critical interactions of MMK3 obtained after applying MD simulations. The hydrogen bonding between the oxygen of the carbonyl ring of pyrrolidinone is now shifted to the amide proton of GLN257. Another hydrogen bonding is observed between the nitrogen of imidazole ring and hydrogen of hydroxyl group of Ser109. The aromatic ring bearing the methoxy group is surrounded by a lipophilic core (Lys199, Asn200 and Tyr184), while the aromatic ring of benzimidazole by the amino acids Val108, Ser109 and Phe110.

3.2. Differential scanning calorimetry

The thermal changes in the pure DPPC/water system as well as the influence of different concentrated inclusions of MMK3 in DPPC bilayers are shown in Fig. 5. Without any drug (top curve) two characteristic endothermic peaks are visible referring to the pre- and the main transition, respectively. The DPPC molecules form below the pre-transition the well organized lamellar gel phase, $L_{\beta'}$ while above the main transition temperature the fluid lamellar phase, L_{α}, is apparent. An intermediate phase, $P_{\beta'}$ is also observed, in which the bilayers are modulated by a periodic ripple (ripple phase). The recorded transition temperatures and enthalpies are in good agreement with literature values [27] (Table 4). In the presence of the drug MMK3 the following observations have been made. Already, at only 1 mol% of MMK3 the pre-transition is suppressed indicating an effect in the head-group regime of the drug molecule. Further, with increasing drug concentration the main transition temperature and the transition cooperativity decrease monotonously. This shows that drug molecules exert an additional effect in the alkyl chains, when the concentration is increased. The enthalpy of the main transition increases slightly from 7.5 to 8.1 kcal/mol for $x = 0.01$ to 0.20 and it is above that of DPPC (7.4 kcal/mol). However, the total ΔH remains below the total enthalpy of the pure DPPC bilayers (8.5 kcal/mol). As we will outline later this enthalpy increase indicates a partial interdigitation of the alkyl chains.

3.3. Raman spectroscopy

Raman spectra of DPPC bilayers alone and in the presence of $x = 0.20$ MMK3 were obtained in a temperature range of 27–50 °C and were recorded in a range of 500–3500 cm^{-1}. In order to characterize the transition behavior, especially the C–C and C–H stretching modes, respectively, have been analyzed in greater detail.
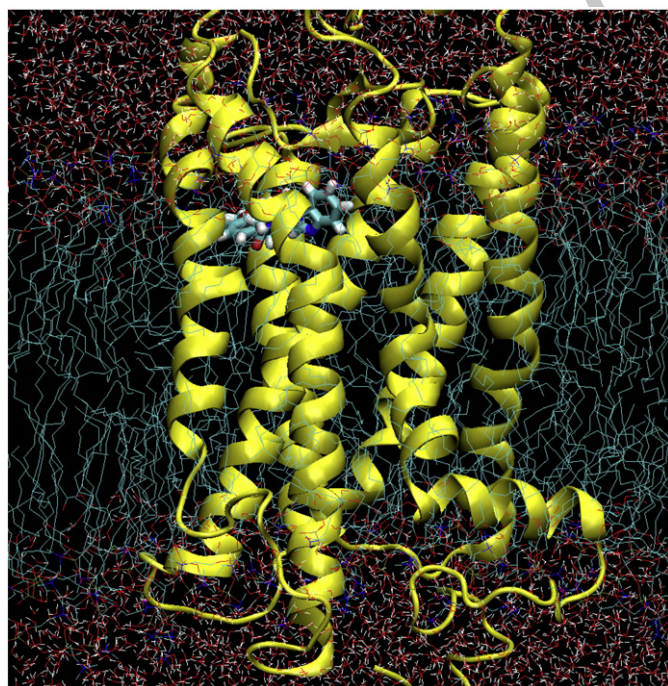
Fig. 3. Docking of MMK3 in AT$_1$ receptor surrounded by lipid bilayers. Yellow color represents the seven helices of AT$_1$ receptor. Lipid bilayers are constituted with 128 DPPC lipids and 3655 waters. (For interpretation of the references to colour in this figure legend, the reader is referred to the web version of this article.)
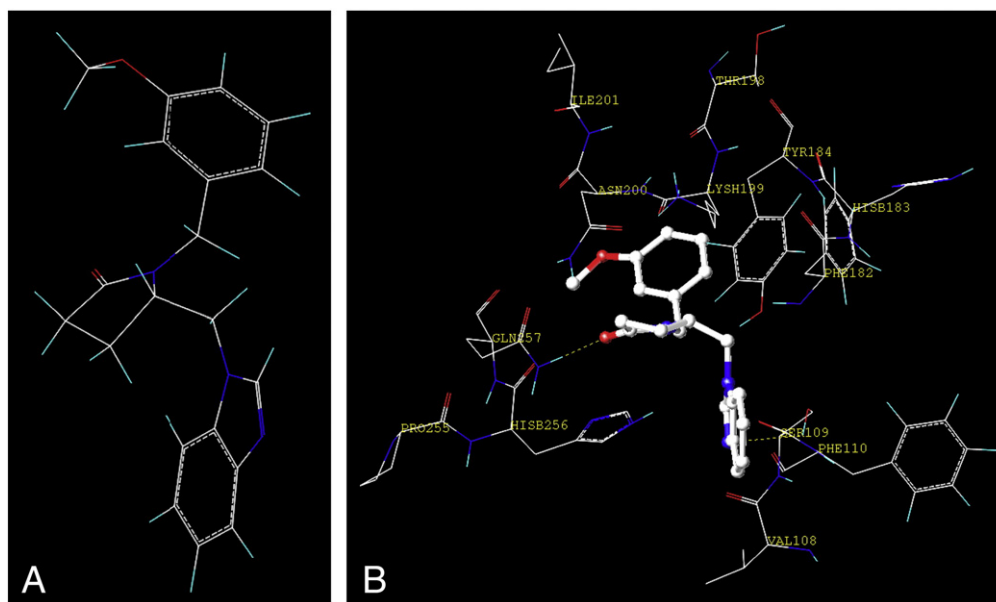
Fig. 4. Panel A shows the conformation of MMK3 before the MD simulations and panel B the critical interactions of MMK3 obtained after applying MD simulations.

The C–C stretching mode region in the 1050–1150 cm^{-1} spectral interval reflects directly intramolecular *trans–gauche* conformational changes within the hydrocarbon chain region of the lipid matrix. Especially, the temperature profiles of the peak height intensity ratio $I_{1090/1130}$ allows the direct comparison of the bilayers disorder–order characteristics between bilayers preparations without or with drug incorporation [34, 35]. Fig. 6 shows the changes in $I_{1090/1130}$ intensity ratio caused by MMK3 when it is incorporated in DPPC bilayers. The transition temperatures compare well to the results found from the calorimetric measurement, and it is clearly seen that MMK3 induces lowering of the *gauche/trans* ratio, i.e. across the gel to fluid phase transition ΔI drops from >0.8 to about 0.2. In summary, the gel phase region displays a greater fluidity in the presence of MMK3 and on the other side, the lipid chains in the fluid chain region exhibit less *trans* to *gauche* isomerizations.

The methylene C–H stretching mode region 2800–3100 cm^{-1} provides the most intense bands in the Raman spectrum of lipid samples and is commonly used to monitor changes in the lateral packing properties and mobility of the lipid chain in both gel and liquid crystalline bilayer systems. In particular, the 2935/2880 intensity ratio measures effects originating from changes both in interchain and intrachain order–disorder processes in the bilayer acyl chains. Although the C–H stretching mode region consists of many superimposed vibrational transitions, the peak height intensity ratio described above provides a sensitive probe to monitor the lipid phase transitions [59–61]. Fig. 7 shows changes in 2935/2880 peak height intensity ratio caused by MMK3, when incorporated in DPPC bilayers. Although the effect is not as strongly expressed as in the $I_{1090/1130}$ intensity ratio, ΔI drops about 20–30% during the gel to fluid phase transition indicating that the entropy changes of the melting is increased under the influence of MMK3.

Other characteristic band alterations give evidence for the incorporation of MKK3 in the DPPC bilayers (data not shown). First, an additional band around 1600 cm^{-1} was observed, which is attributed to an alteration of the stretch vibration of the amide bond. Second, at 714 cm^{-1} corresponding to C–N stretch vibration, a shift to
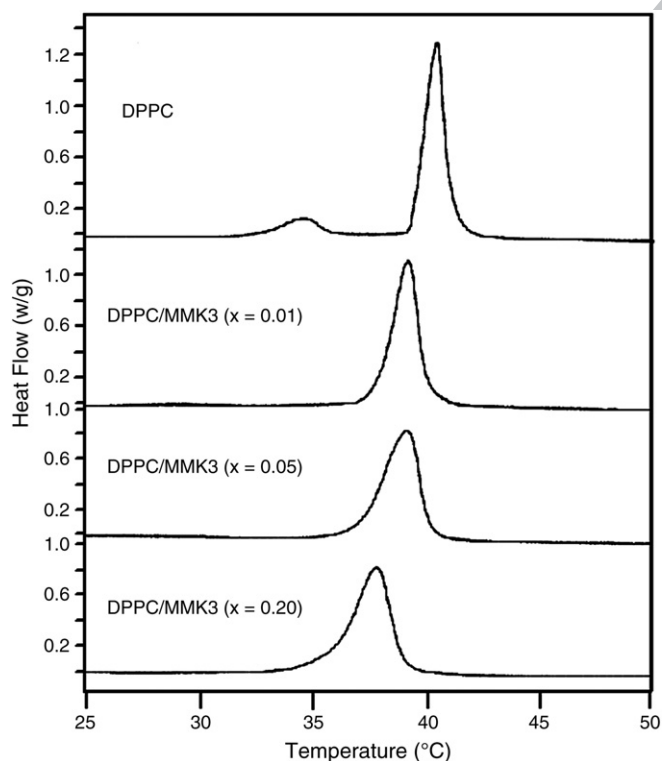

Fig. 5. DSC scans of DPPC bilayers containing MMK3 at molar ratios $x = 0.01$, 0.05 and 0.20. The thermal scan attributed to DPPC bilayers shows two distinct thermal events. The incorporation of the drug eliminates the small endothermic event (pre-transition). The higher the incorporated concentration of the drug, the broader the transition width and the lower the phase transition temperature.

Table 4

T_{onset}, T_m, $T_{m1/2}$ and ΔH of DPPC alone and with incorporated MMK3 at molar ratios $x = 0.01$, 0.05 and 0.20.

Samples	T_{onset} (°C)	T_m (°C)	$T_{m1/2}$ (°C)	ΔH (kcal/mol)
DPPC	(32.1) 39.4	(35.9) 41.2	(2.0) 1.0	(1.12±0.07) 7.36±0.05
DPPC/MMK3 ($x = 0.01$)	38.7	40.2	1.3	7.50±0.07
DPPC/MMK3 ($x = 0.05$)	38.0	40.0	1.8	7.88±0.10
DPPC/MMK3 ($x = 0.20$)	36.7	38.6	1.8	8.10±0.17

Values in brackets are given for the pre-transition of DPPC. The table refers to experiments displayed in Fig. 5.
R data (compare also Tables 2 and 3).

418 higher values was observed, when MMK3 is present in the membrane.
419 This indicates that MMK3 interacts with head-groups. Third, MMK3
420 caused a shift and line-shape changes at 1296 cm^{-1}, which
421 correspond to stretching vibrations of the $(CH)_2$ region of the DPPC
422 bilayers. This is a direct evidence of the interaction of MMK3 with
423 $(CH)_2$ region of the DPPC bilayers.

424 ### 3.4. X-ray diffraction

425 Static small angle X-ray scattering experiments were carried out
426 on DPPC/MKK3 multilamellar vesicles to elucidate the influence of the
427 drug onto the model membrane system (Fig. 8). Remarkably, already
428 in the gel phase, MMK3 has a strong influence on the DPPC
429 membranes. Visible by naked eye the usually observed quasi long
430 range order of the membrane stacking is not preserved any more.
431 Instead of recording the first five diffraction peaks as seen for pure
432 DPPC liposomes in the gel phase [62], only the first order reflection is
433 relatively well expressed (Fig. 8A). The global fitting analysis reveals
434 two reasons for the rather diffuse scattering pattern. First, the
435 averaged number of correlated membranes is very low, i.e. the
436 crystallite size is limited to only about 3 lamellae, and second, the root
437 mean square fluctuation σ of the membranes is about 3 times higher
438 than normal (Table 5). The bilayer thickness as seen in the
439 corresponding electron density profile (Fig. 8C) is only slightly
440 influenced by the presence of MKK3, whereas the inter-membrane
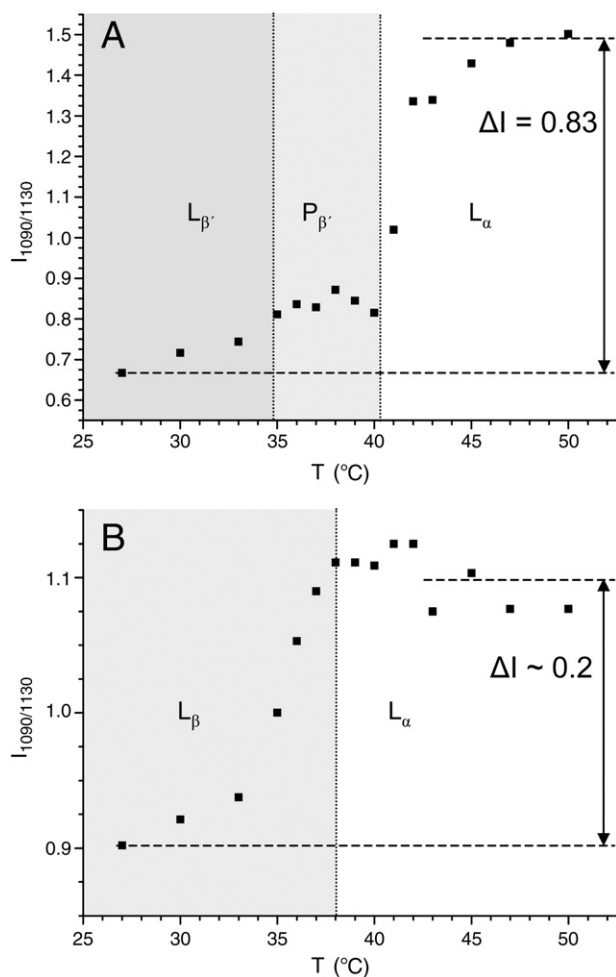441 distance is about 7 Å increased when compare to the pure DPPC/

water system (Table 5). In the fluid lamellar phase at 50 °C the 442
diffraction pattern appears common (Fig. 8B): the quasi long range 443
order and the root mean square fluctuation σ in the multilamellar 444
system are very similar to those found in pure DPPC [63–67] (Table 5). 445
However, the fitting results show that the bilayer thickness is clearly 446
reduced (about −4 Å) (Fig. 8D). 447

Fig. 7. $I_{2935/2880}$ vs. temperature graphs for (A) DPPC alone and (B) DPPC bilayers containing $x = 0.20$ of MMK3. Note, that the presence of drug lowers the phase transition temperature in agreement with DSC data (Fig. 5).

4. Discussion 448

MMK3 is a synthetic molecule designed rationally to mimic the 449
antihypertensive effects of AT_1 antagonists. Its lower activity 450
relatively to the prototype of AT_1 antagonist losartan led us to study 451
thoroughly its conformational properties both in the receptor site and 452
in a lipid environment. MMK3 fits nicely within the active site of the 453
cavity as reported for other AT_1 antagonists [68]. However, it does not 454
tightly interact with critical amino acids of Lys199 and His256 as it is 455
reported with the AT_1 antagonists. This may explain in part its 456
relatively low activity. 457

Since AT_1 antagonists act in the active site of AT_1 receptor localized 458
in the transmembrane segment, we postulated an important role in 459
their action with the membrane itself. For this reason, we have also 460
studied the effects of MMK3 within lipid bilayers to reveal their 461
possible role in the drug action. 462

DSC results showed that already at low concentrations ($x = 0.01$) 463
MMK3 as losartan suppresses the pre-transition, a first hint for its 464
polar interface activity. At higher concentrations MMK3 causes T_m 465
lowering, decrease of cooperativity and slight increase of enthalpy 466

Fig. 6. $I_{1090/1130}$ vs. temperature graphs for (A) DPPC alone and (B) DPPC bilayers containing $x = 0.20$ of MMK3. Note, that the presence of drug lowers the phase transition temperature and decreases ΔI, which is accompanied with a broadening of phase transition temperature in agreement with DSC data (Fig. 5).
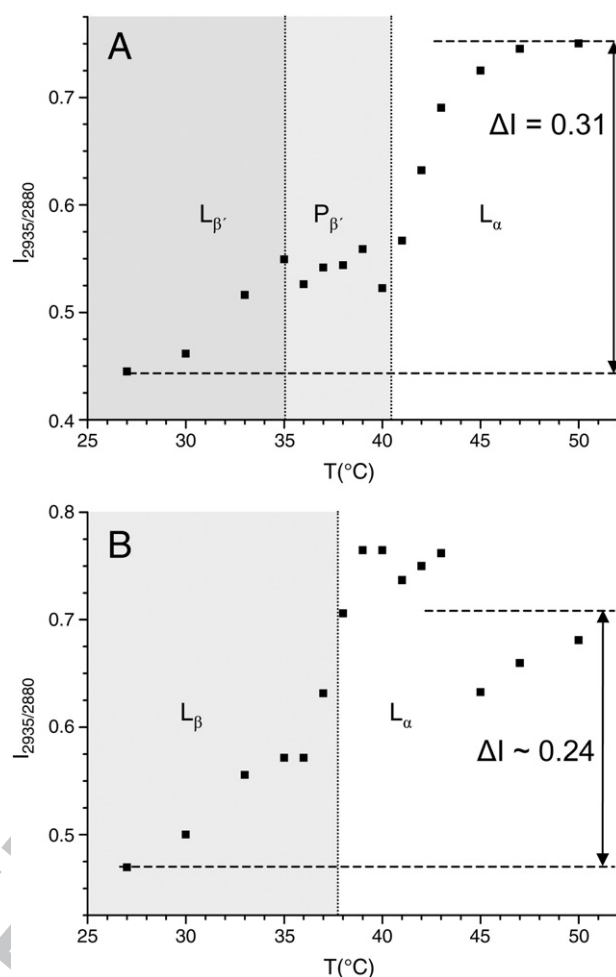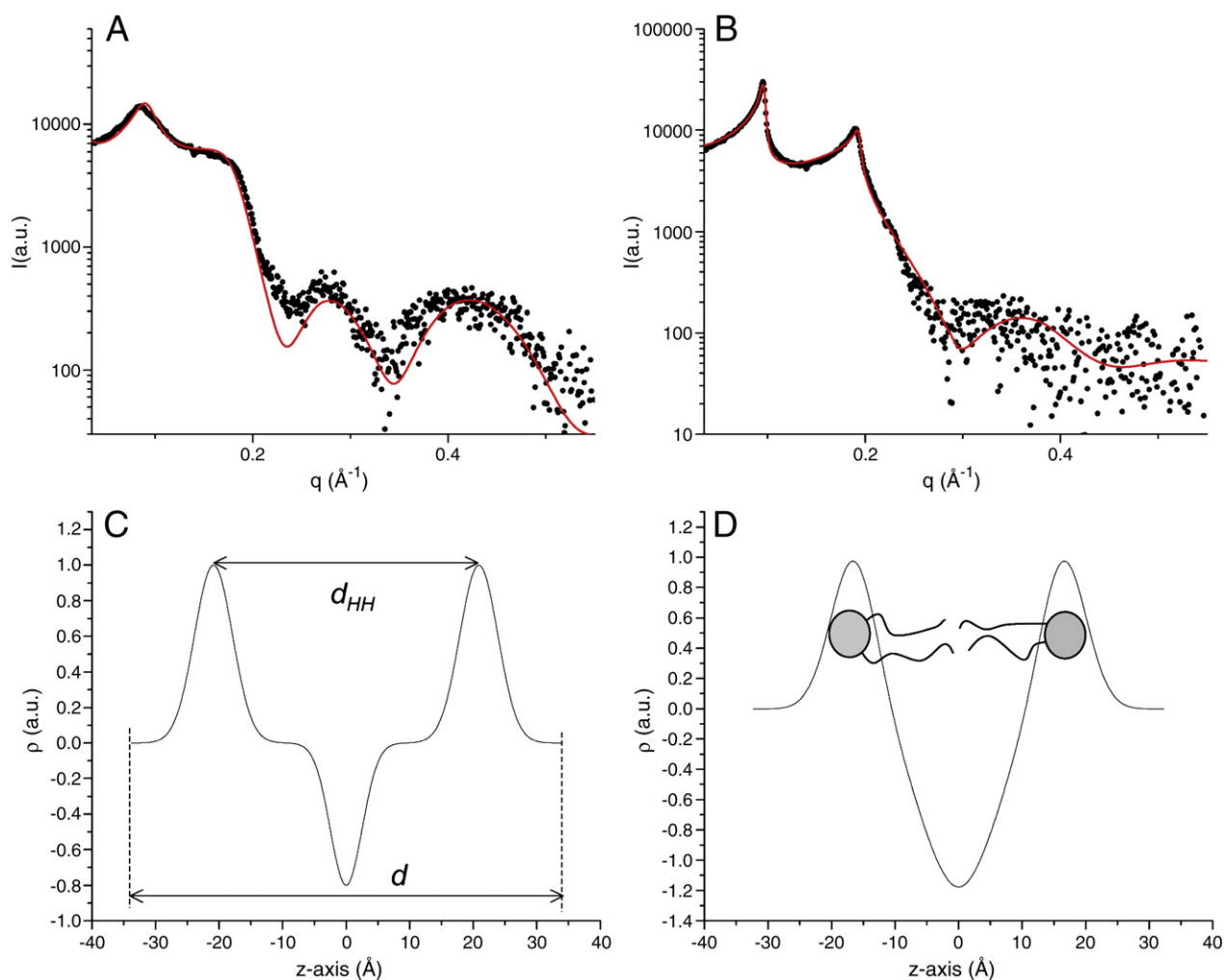
Fig. 8. X-ray scattering curves of DPPC/MMK3 multilamellar vesicles at 25 °C (A) and 50 °C (B), and their corresponding electron density profiles (C), (D). (Top) The full red lines give the global fit to the data. (Bottom) d_{HH} defines the head to head-group distance and d the lattice repeat distance. For clarity in panel D two lipid molecule models are superimposed to the electron density profile of the bilayer. The most significant structural parameters are summarized in Table 5. (For interpretation of the references to colour in this figure legend, the reader is referred to the web version of this article.)

change of main transition. AT_1 antagonist losartan has shown to exert similar, but more pronounced, thermal effects on DPPC bilayers [69]. T_m values of DPPC bilayers containing losartan at identical concentrations of $x = 0.05$ and $x = 0.20$ are 38.9 and 35.3 °C, respectively, and are lower as compared to values of 40.0 and 38.6 °C observed in bilayers containing MMK3. ΔH for DPPC bilayers containing $x = 0.05$ of either MMK3 or losartan is identical, but at higher concentration of $x = 0.20$ ΔH is higher for the bilayers containing losartan. This indicates that both drugs either significantly increase the *trans:gauche* isomerization and/or enhance the van der Waals interactions during the main phase transition with losartan being more effective.

Table 5
Structural data on pure DPPC bilayers and DPPC with 20 mol% MMK3 ($x = 0.20$).

|	DPPC (20 °C)	DPPC (50 °C)	DPPC/MMK3 (25 °C)	DPPC/MMK3 (50 °C)
d (Å)	63.5[a]	67.0[a]	67.7	64.7
d_{HH} (Å)	44.2[a]	38.3[a]	42	33
$d - d_{HH}$ (Å)	19.3[a]	28.7[a]	26	32
σ (Å)	1[b]	6[c]	3	7

[a] Structural data taken from the review [12].
[b] Estimated value from global data analysis (data not shown).
[c] Data concerning the root mean square fluctuation in pure DPPC rely on data from [10,11].

Raman Spectroscopy results confirmed and complemented those obtained by DSC. In particular, Raman results showed that the gel phase in the presence of MMK3 appeared more fluid and the fluid phase less fluid in comparison with DPPC bilayers alone. The *trans: gauche* isomerization reduction points out that the enthalpy increase observed in DSC experiments is solely attributed to the increase of van der Waals interactions, giving a hint of partial interdigitation effect. Again, similar but more pronounced results are obtained with DPPC bilayers containing losartan [69].

X-ray diffraction results show that incorporated MMK3 enhances the inter-membrane distance, $d - d_{HH}$, in a range from 4 to 7 Å (see Table 5), inducing some additional steric repulsion between adjacent membranes. Possibly, throughout its interfacial activity it softens the bilayer and hence causes increased undulation of the membrane. This view is further supported by the observed increase of the root mean square fluctuation σ especially in the gel phase (25 °C). The analysis of membrane thickness reveals a different picture, here the main changes take place in the fluid lamellar phase, i.e. the bilayer reduces about 4 Å in the presence of MMK3. A possible interpretation is outlined in Fig. 9. Throughout the insertion of MMK3 into on leaflet of the membrane voids are induced that need to be filled by lipids of the opposite leaflet. This in turn causes neighboring lipid molecules to interdigitate partially. We note that the scheme bases on experimental X-ray data, i.e. the decomposition
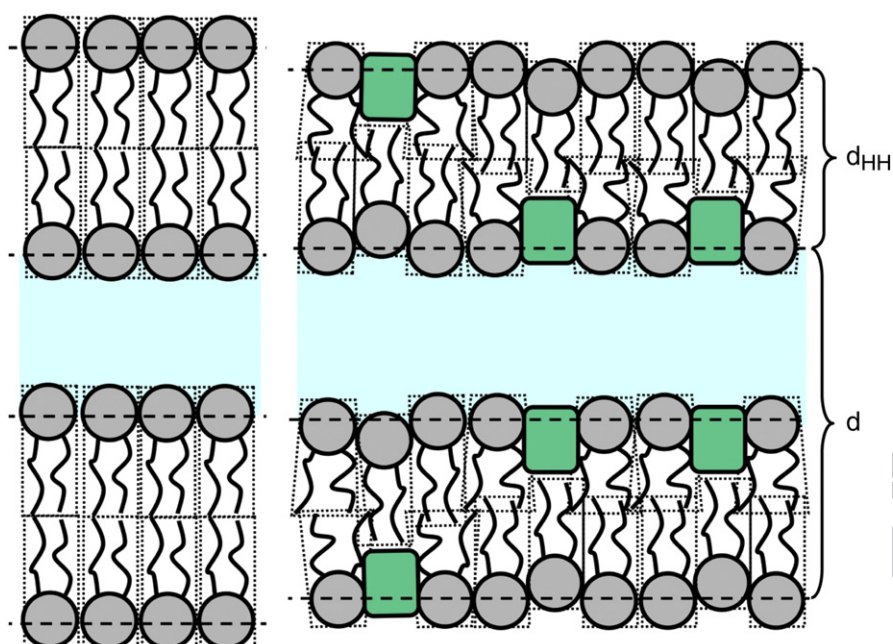
Fig. 9. Bilayer stacking in pure DPPC (left) and DPPC/MMK3 multilamellar vesicles (right). The structural data are summarized in Table 5. The rough size of the MMK3 drug has been estimated from NMR data (compare also Tables 2 and 3).

of the d-spacing into bilayer and water layer thickness is realistic both for the pure DPPC/water as well as for the DPPC-MMK3/water system.

Thus, taken all complementary results of DSC, Raman spectroscopy and X-ray diffraction together, we proved the induction of partial interdigitation in the liquid crystalline phase for the first time. Within this interpretation all experimental results are consistent. First, the enthalpy increase is caused by an increase difference of the van der Waals interactions between gel and liquid crystalline phases. Second, the $trans:gauche$ isomerization reduction during the main transition precludes the observed thinning of the fluid bilayer to be due to the effective lipid length shortening. Third, the overall thinning of the membrane can be sufficiently explained by partial interdigitation as demonstrated in Fig. 9.

We have already reported that partial interdigitation is observed for the bulky molecule of vinblastine and the antihypertensive AT_1 antagonist losartan. Both molecules are characterized as amphiphiles that reside on the interface regime and possess net positive and negative charges. These charges may be responsible for their stronger anchoring in this region and cause more effective partial interdigitation effect [70–72].

In conclusion, we showed that MMK3's observed lower bioactivity in comparison to SARTANs may be attributed mainly to two reasons: first, although it resides at the interface regime of lipid bilayers in the same manner as SARTANs do, its thermodynamical and structural effects are not as pronounced. This may preclude MMK3 to reach the critical concentration for reaching the active site of the receptor. Second, although the drug molecule fits nicely to the active site of the receptor, it does not exert the right interactions with the key amino acids lacking the proper stereoelectronic requirements. Therefore, MMK3's Odyssey to Ithaca is restrained by two elements: the nature of the bilayer matrix and stereoelectronic active site requirements.

To further examine the role of the lipid bilayers we are currently performing similar studies with other AT_1 antagonists. Hitherto, such studies show that AT_1 antagonists do not exert a unique perturbing effect, and hence, these results urge for more comprehending understanding of the role of lipid bilayers in the antihypertensive drug action.

In this respect, we like to point out that there is a growing awareness that even small structural variations in the composition of cell membranes can influence the function of intrinsic membrane proteins. Any membrane active drug does change the lateral pressure profile in bilayers and hence, can affect the behavior of membrane proteins [73]. This means that at least locally any membrane interface active solute leaves its special fingerprint [74], and it will be of great importance for future rational drug design to understand not only direct drug action at the active site, but also to understand specific drug to bilayer interactions to foresee at least qualitatively the consequences for drug efficiency.

References

[1] J.L. Pool, R.E Schmieder, M. Azizi, J.C. Aldigier, A. Januszewicz, W. Zidek, Y. Chiang, A. Satlin, Aliskiren, an orally effective rennin inhibitor, provides antihypertensive efficacy alone and in combination with valsartan, Am. J. Hypert. 20 (2007) 11–20.

[2] M. De Gasparo, K.J. Catt, T. Inagami, J.W. Wright, T. Ugner, The angiotensin II receptors, Pharmacol. Rev. 52 (2000) 415–472.

[3] C. Sakarellos, K. Lintner, F. Piriou, S. Fermandjian, Conformation of the central sequence of angiotensin II and analogs, Biopolymers 22 (1983) 663–687.

[4] J.M. Matsoukas, J. Hondrelis, M. Keramida, T. Mavromoustakos, A. Makriyannis, R. Yamdagni, Q. Wu, G. Moore, Role of the NH2-terminal domain of ANG II and [Sar1] ANG II on conformation and activity: NMR evidence for aromatic ring clustering and peptide backbone folding compared to [Des1,2,3] ANG II, J. Biol. Chem. 269 (1994) 5303–5312.

[5] E. Theodoropoulou, T. Mavromoustakos, D. Panagiotopoulos, J. Matsoukas, J. Smith, Superimposition of potent non-peptide AT1 receptor antagonists with angiotensin II, Lett. Pept. Sci. 3 (1996) 209–216.

[6] J.M. Matsoukas, L. Polevaya, J. Ancas, T. Mavromoustakos, A. Kolocouris, P. Roumelioti, D.V. Vlahakos, R. Yamdagni, Q. Wu, G.J. Moore, The design and synthesis of a potent angiotensin II cyclic analogue confirms the ring cluster receptor conformation of the hormone angiotensin II, Bioorg. Med. Chem. Lett. 8 (2000) 1–10.

[7] P. Roumelioti, T. Tselios, K. Alexopoulos, T. Mavromoustakos, A. Kolocouris, G.J. Moore, J.M. Matsoukas, Structural comparison between type I and type II antagonists: in the drug design of AT-1 antagonists, Bioorg. Med. Chem. Lett. 10 (2000) 755–758.

[8] L. Polevaya, T. Mavromoustakos, P. Zoumboulakis, S.G. Grdadolnik, P. Roumelioti, N. Giatas, I. Mutule, T. Keivish, D. Vlahakos, E. Iliodromitis, D. Kremastinos, Synthesis and study of cyclic angiotensin II antagonist analogue reveals the role of π*–π* interactions in the C-terminal aromatic residue for agonist activity and its structure resemblance with AT1 non-peptide antagonists, Bioorg. Med. Chem. 9 (2001) 1639–1647.

[9] P. Roumelioti, L. Polevaya, P. Zoumpoulakis, N. Giatas, T. Keivish, A. Haritonova, A. Zoga, D. Vlahakos, E. Iliodromitis, D. Kremastinos, S.G. Grdadolnik, T. Mavromoustakos, J.M. Matsoukas, Design, synthesis and biological evaluation of cyclic angiotensin II analogues with 3,5 side chain bridges: role of C-terminal

aromatic residue and ring cluster for activity and implications in the drug design of AT1 non peptide antagonists, Bioorg. Med. Chem. Lett. 12 (2002) 2627–2633.

[10] M.A.C. Preto, A.M. Hermani, L.S. Maia, T. Mavromoustakos, M.J. Ramos, Molecular dynamics simulations of angiotensin II in aqueous and dimethylsulfoxide environments, J. Phys. Chem. B 109 (2005) 17743–17751.

[11] J.M. Matsoukas, G. Agelis, A. Wahhab, J. Hondrelis, D. Panagiotopoulos, R. Yamdagni, Q. Wu, T. Mavromoustakos, H.L.S. Maia, R. Ganter, G.J. Moore, Differences in backbone structure between angiotensin II agonists and type I antagonists, J. Med. Chem. 38 (1995) 4660–4669.

[12] T. Mavromoustakos, E. Theodoropoulou, C. Dimitriou, J. Matsoukas, D. Panagiotopoulos, A. Makriyannis, Interactions of angiotensin II with membranes using a combination of differential scanning calorimetry and 31P-NMR spectroscopy, Lett. Pept. Sci. 3 (1996) 175–180.

[13] T. Mavromoustakos, A. Kolocouris, M. Zervou, P. Roumelioti, J. Matsoukas, R. Weisemann, An effort to understand the molecular basis of hypertension through the study of conformational analysis of losartan and sarmesin using a combination of Nuclear Magnetic Resonance spectroscopy and theoretical calculations, J. Med. Chem. 42 (1999) 1714–1722.

[14] P. Zoumpoulakis, S.G. Grdadolnik, J.M. Matsoukas, T. Mavromoustakos, Structure elucidation and conformational properties of eprosartan a non peptide Angiotensin II AT1 antagonist, J. Pharm. Biomed. Anal. 28 (2002) 125–135.

[15] P. Zoumpoulakis, A. Zoga, P. Roumelioti, N. Giatas, S.G. Grdadolnik, E. Iliodromitis, D. Vlahakos, D. Kremastinos, J.M. Matsoukas, T. Mavromoustakos, Conformational and biological studies for a pair of novel synthetic AT1 antagonists. Stereoelectronic requirements for antihypertensive efficacy, J. Pharm. Biomed. Anal. 31 (2003) 833–844.

[16] P. Zoumpoulakis, A. Politi, S.G. Grdadolnik, J.M Matsoukas, T. Mavromoustakos, Structure elucidation and conformational study of V8. A novel synthetic non peptide AT1 antagonist, in press, J. Pharm. Biomed. Anal. 40 (2006) 1097–1104.

[17] T. Mavromoustakos, P. Zoumpoulakis, I. Kyrikou, A. Zoga, E. Siapi, M. Zervou, I. Daliani, D. Dimitriou, A. Pitsas, C. Kamoutsis, P. Laggner, Efforts to understand the molecular basis of hypertension trough drug:membrane interactions, Curr. Top. Med. Chem. 4 (2004) 445–459.

[18] T. Mavromoustakos, M. Zervou, P. Zoumpoulakis, I. Kyrikou, N.P. Benetis, L. Polevaya, P. Roumelioti, N. Giatas, A. Zoga, P.M. Minakakis, A. Kolocouris, D. Vlahakos, S.G. Grdadolnik, J.M Matsoukas, Conformation and bioactivity. Design and discovery of novel antihypertensive drugs, Curr. Top. Med. Chem. 4 (2004) 385–401.

[19] P.M. Minakakis, M. Gianni, H. Stougiannou, P. Zoumpoulakis, A. Zoga, A.D. Vlahakos, E. Iliodromitis, T. Mavromoustakos, Design and synthesis of novel antihypertensive drugs, Bioorg. Med. Chem. Lett 13 (2003) 1737–1740.

[20] T. Mavromoustakos, P.M. Minakakis, C.G. Kokotos, P. Kontogianni, A. Politi, P. Zoumpoulakis, J. Findlay, A. Cox, A. Balmforth, A. Zoga, E. Iliodromitis, Synthesis, binding studies, and in vivo biological evaluation of novel non-peptide antihypertensive analogs, Bioorg. Med. Chem. 14 (2006) 4353–4360.

[21] P. Zoumpoulakis, I. Daliani, M. Zervou, I. Kyrikou, E. Siapi, G. Lamprinidis, E. Mikros, T. Mavromoustakos, Losartan's molecular basis of interaction with membranes and AT1 receptor, Chem. Phys. Lipids 125 (2003) 13–25.

[22] L.G. Herbette, Pharmacokinetic and pharmacodynamic design of lipophilic drugs based on a structural model for drug-interactions with biological membranes, J. Pestic. Sci. 35 (1992) 363–368.

[23] H.S Young V. Skita, R.P. Mason, L.G. Herbette, Molecular-basis for the inhibition of 1,4-dihydropyridine calcium-channel drugs binding to their receptors by a non-specific site interaction mechanism, Biophys. J. 61 (1992) 1244–1255.

[24] D.G. Rhodes, R. Newton, R. Butler, L. Herbette, Equilibrium and kinetic studies of the interactions of selmetrol with membrane bilayers, Mol. Pharmacol. 42 (1992) 596–602.

[25] T. Mavromoustakos, D.P. Yang, A. Makriyannis, Small angle X-ray diffraction and differential scanning calorimetric studies on O-methyl-(−)-Δ8-Tetrahydrocannabinol and its 5′ iodinated derivative in membrane bilayers, Biochim. Chemistry Acta 1237 (1995) 183–188.

[26] T. Tuccinardi, P.L. Ferrarini, C. Manera, G. Ortore, G. Saccomanni, A. Martinelli, Cannabinoid CB2/CB1 selectivity. Recep-1118 tor modeling and automated docking analysis, J. Med. Chem. 49 (2006) 984–994.

[27] K. Rumiana, M. Caffrey, Phases and phase transitions of the phosphatidylcholines, Biochim. Biophys. Acta 1376 (1998) 91–145.

[28] S. Tristram-Nagle, M.C. Wiener, C.P. Yang, J.F. Nagle, Kinetics of the subtransition in diplamitoylphosphatidylcholine dispersions, Biochemistry 26 (1987) 4288–4294.

[29] M.D. Houslay, K.K. Stanley, Dynamics of Biological Membranes, John Wiley and Sons, New York, 1982.

[30] R.P. Rand, D. Chapman, K. Larsson, Tilted hydrocarbon chains of dipalmitoyl lecithin become perpendicular to the bilayer before melting, Biophys. J. 15 (1975) 1117–1124.

[31] J. Stamatoff, B. Feuer, H.J. Guggenheim, G. Tellez, T. Yamane, Amplitude of rippling in the PB phase of dipalmitoylphosphatidylcholine bilayers, Biophys. J. 38 (1982) 217–226.

[32] T.J. McIntosh, Differences in hydrocarbon chain tilt between hydrated phosphatidylethanolamine and phosphatidylcholine bilayers: a molecular packing model, Biophys. J. 29 (1980) 237–246.

[33] N.B. Colthup, L.H. Daly, S.E. Wiberley, Introduction to Infrared and Raman Spectroscopy, Third Ed. Academic Press, New York, 1990.

[34] C. Huang, J.R. Lapides, I.W. Levin, Phase-transition behaviour of saturated, symmetric chain phospholipid bilayers dispersions determined by Raman spectroscopy: correlation between spectral and thermodynamic parameters, J. Am. Chem. Soc. 104 (1982) 5926–5930.

[35] I.W. Levin, E.N. Lewis, Fourier transform Raman spectroscopy of biological materials, Anal. Chem. 62 (1990) 1101A–1111A.

[36] G. Pabst, M. Rappolt, H. Amenitsch, P. Laggner, Structural information from multilamellar liposomes at full hydration: full q-range fitting with high quality X-ray data, Phys. Rev. E 62 (2000) 4000–4009.

[37] T.J. Netticadan, T.F. Ashavaid, K.G. Nair, Characterisation of the canine cardiac sarcolemma in experimental mzocardial ischemia, Indian J. Clin. Biochem. 12 (1) (1997) 49–54.

[38] M. Trumbore, W. Chester, J. Moring, D. Rhodes, Structure and location of amiodarone in a membrane bilayer as determined by molecular mechanics and quantitative X-ray diffraction, Biophys. J. 54 (1988) 535–543.

[39] C. Griesinger, R.R. Ernst, Frequency offset effects and their elimination in NMR rotating-frame cross-relaxation spectroscopy, J. Magn. Reson. 75 (1987) 261–271.

[40] Sybyl Molecular Modeling Software Package ver. 6.8; Tripos Inc.: St. Louis, MO 63144, 2001.

[41] A.W. Schuettelkopf, D.M.F. van Aalten, A tool 1049 for high-throughput crystallography of protein–ligand complexes, Acta Cryst.D 60 (2004) 1355–1363.

[42] M. Patra, M. Karttunen, M. Hyvönen, E. Falck, P. Vattulainen, Lipid bilayers driven to a wrong lane in molecular dynamics simulations by subtle changes in long-range electrostatic interactions, J. Phys. Chem. B 108 (2004) 4485–4494.

[43] M. Patra, M. Karttunen, M. Hyvonen, E. Falck, P. Lindqvist, I. Vattulainen, Molecular dynamics simulations of lipid bilayers: major artifacts due to truncating electrostatic interactions, Biophys. J. 84 (2003) 3636–3645.

[44] E. Lindhal, B. Hess, D. van der Spoel, GROMACS 3.0: a package for molecular simulation and trajectory analysis, J. Mol. Model. 7 (2001) 306–317.

[45] W.F. van Gunsteren, S.R. Billeter, A.A. Eising, P.H. Hunenberger, P. Kruger, A.E. Mark, W.R.P. Scott, I.G. Tironi, Biomolecular simulation: the GROMOS96 manual and user guide, Vdf Hochschulverlag AG an der ETH Zurich, Zurich, 1996.

[46] H.J.C. Berendsen, J.P.M. Postma, W.F. van Gunsteren, A. Dinola, J.R. Haak, Molecular dynamics with coupling to an external bath, J. Comput. Chem. 81 (1984) 3684–3690.

[47] U. Essmann, L. Perera, M.L. Berkowitz, T. Darden, H. Lee, L.G. Pedersen, A smooth particle mesh Ewald method, J. Chem. Phys. 103 (1995) 8577–8592.

[48] M. Parrinello, A. Rahman, Polymorphic transitions in single crystals: a new molecular dynamics method, Jpn. J. Appl. Phys. 52 (1981) 7182–7190.

[49] B. Hess, H. Bekker, H.J.C. Berendsen, J.G.E.M. Fraaije, LINCS: a linear constraint solver for molecular simulations, J. Comput. Chem. 18 (1997) 1463–1472.

[50] W. Humphrey, A. Dalke, K. Schulten, VMD: visual molecular dynamics, J. Mol. Graph. 14 (1996) 33–38.

[51] P. Laggner, H. Mio, SWAX, a dual-detector camera for simulations small and wide-angle X-ray diffraction in polymer and liquid crystal research, Nucl. Instrum. Methods, Phys. Res. A 323 (1992) 86–90.

[52] G. Pabst, M. Rappolt, H. Amenitsch, P. Laggner, Structural information for multilamellar liposomes at full hydration: full q-range fitting with high-quality X-ray data, Phys. Rev. E 62 (2000) 4000–4009.

[53] A. Caillé, Remarques sur la diffusion des rayons X dans les smectiques, A. C. R. Acad. Sci. Sér. B 274 (1972) 891–893.

[54] R. Zhang, N.S. Tristram, W. Sun, R.L. Headrick, T.C. Irving, R.M. Suter, J.F. Nagle, Small-angle X-ray scattering from lipid bilayers is well described by modified Caillé theory but not by paracrystalline theory, Biophys. J. 70 (1996) 349–357.

[55] R. Hosemann, S.N. Bagchi, Direct Analysis of Diffraction by Matter, North-Holland publishing Co, Amsterdam, 1962.

[56] G. Pabst, Global properties of biomimetic membranes: perspectives on molecular features, Biophys. Rev. Lett. 1 (2006) 57–84.

[57] A. Siarheyeva, J.J. Lopez, C. Glaubitz, Localization of multidrug transporter substrates with model membranes, Biochemistry 45 (2006) 6203–6211.

[58] T. Mavromoustakos, M. Zervou, P. Zoumpoulakis. Design and discovery of novel antihypertensive drugs through conformation and bioactivity studies. Bentham Science Publishers Ltd. Co-Editors:Atta-ur-Rahman, Allen B. Reitz. Associate Editors: M. Iqbal Choundhary, Cheryl P. Kordik. Ur Frontiers in Medicinal Chemistry 3 (2006), 87–113.

[59] J.R. Silvius, M. Lyons, P.L Yeagle, T.J. O'Leary, Thermotropic properties of bilayers containing branched-chain phospholipids, calorimetric, Raman and 31P NMR studies, Biochemistry 24 (1985) 5388–5395.

[60] T.J. O' Leary, P.D. Ross, I.W Levin, Effects of anaesthetic and nonanaesthetic steroids on dipalmitoylphosphatidylcholine liposome: a calorimetric and Raman spectroscopic investigation, Biochemistry 23 (1984) 4636–4641.

[61] T.J. O' Leary, I.W. Levin, Raman spectroscopic study of an interdigitated lipid bilayer dipalmitoylphosphatidylcholine dispersed in glycerol, Biochim. Biophys. Acta 776 (1984) 185–189.

[62] M.C. Wiener, R.M. Suter, J.F. Nagle, Structure of the fully hydrated gel phase of diplamitoylphosphatidylcholine, Biophys. J. 55 (1989) 315–325.

[63] J.W. Torbet, M.H.F. Wilkins, X-ray diffraction studies of lecithin bilayers, J. Theor. Biol. 62 (1976) 447–458.

[64] T.J. McIntosh, S.A. Simon, Hydration force and bilayer deformation: a reevaluation, Biochemistry 25 (1986) 4048–4066.

[65] H.I. Petrache, N. Gouliaev, N.S. Tristram, R. Zhang, R.M. Suter, J.F. Nagle, Interbilayer interactions from high-resolution X-ray scattering, Phys. Rev. E 57 (1998) 7014–7024.

[66] G. Pabst, H. Amenitsch, D.P. Kharakoz, P. Laggner, M. Rappolt, Structure and fluctuations of phosphatidylcholines in the vicinity of the main phase transition, Phys. Rev. E 70 (2004) 021908.

[67] J.F. Nagle, N.S. Tristram, Structure of lipid bilayers, Biochim. Biophys. Acta 1469 (2000) 159–195.

[68] C. Potamitis, M Zervou, V. Katsiaras, P Zoumpoulakis, S. Durdagi, M. Papadopoulos, J. Hayes, S. Grdadolnik, I. Kyrikou, D. Argyropoulos, G. Vatougia, T. Mavromoustakos,

758 Antihypertensive drug valsartan in solution and at the AT_1 receptor: conforma-
759 tional analysis, dynamic NMR spectroscopy, in silico docking and molecular
760 dynamics simulations, J. Chem. Inf. Mod. 49 (2009) 726–739.
761 [69] C. Photakis, D. Christodouleas, P. Chatzigeorgiou, M. Zervou, N.P. Benetis, K. Vyras,
762 T. Mavromoustakos, Application of a novel CP-31P NMR methodology to study the
763 possible interdigitation effect of losartan in phospholipids bilayers. Comparison
764 with Raman spectroscopy data, Biophys. J. 96 (2009) 2227–2236.
765 [70] I. Kyrikou, I. Daliani, T. Mavromoustakos, H. Maswadeh, C. Demetzos, S.
766 Xatziantoniou, S. Giatrellis, G. Nounesis, The modulation of thermal and dynamic
767 properties of vinblastine by cholesterol in membrane bilayers, Biochim. Biophys.
768 Acta 1661 (2004) 1–8.

769 [71] H. Maswadeh, C. Demetzos, I. Daliani, I. Kyrikou, T. Mavromoustakos, A. Tsortos, G.
770 Nounesis, A molecular basis explanation of the dynamic and thermal effects of
771 vinblastine sulfate upon dipalmitoylphosphatidylcholine bilayer membranes,
772 Biochim. Biophys. Acta 1567 (2002) 49–55.
773 [72] I. Kyrikou, S. Xadjikakou, D.D. Kovala, K. Viras, T. Mavromoustakos, Effects of non
774 steroid anti-inflammatory drugs in membrane bilayers containing cholesterol,
775 Chem. Phys. Lipids 132 (2004) 157–169.
776 [73] R.S. Cantor, The lateral pressure profile in bilayers, Biophys. J. 76 (1999) 2625–2639.
777 [74] C. Xing, O.H.S. Ollila, I. Vattulainen, R. Olli, Asymmetric nature of lateral pressure
778 profiles in supported lipid membranes and its implications for membrane protein
779 functions, Soft Matter 5 (2009) 3258–3261.

780